Journal of Materials Chemistry A

Accepted Manuscript

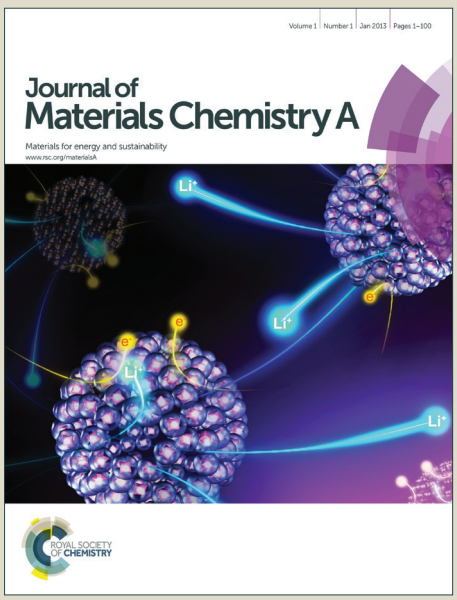

ROYAL SOCIETY OF CHEMISTRY

www.rsc.org/materialsA

Thermoelectric properties of pulsed current sintered nanocrystalline Al-doped ZnO by chemical vapour synthesis

D. Gautam*, M. Engenhorst, C. Schilling, G. Schierning, R. Schmechel and M. Winterer

Faculty of Engineering and Center for Nanointegration Duisburg-Essen (CENIDE), University of Duisburg-Essen, 47057 Duisburg, Germany

*e-mail: devendraprakash.gautam@uni-due.de

Abstract

ZnO is a promising *n*-type oxide thermoelectric material, which is stable in air at elevated temperatures. In the present study we report the bottom-up approach to create Al-doped ZnO nanocomposites from nanopowders, which are prepared by chemical vapour synthesis. With our synthesis route we are able to create highly doped Al-containing ZnO nanocomposites that exhibit bulk like electrical conductivity. Concurrently, the impact of microstructure of nanocomposites on their thermal conductivity is enormous with a value of 1.0 W/mK for 1% Al-ZnO at room temperature, which is one of the lowest values reported so far on ZnO nanocomposites. The optimization of the Al-doping and microstructure with respect to the transport properties of bulk Al-ZnO nanocomposites leads to a zT value of about 0.24 at 950 K, underlining the potential of our technique.

Introduction

Nanostructured materials based on alloys, namely; tellurides, skutterudites, transition-metal silicides and Si-Ge alloys exhibit good thermoelectric properties.[1, 2] However, their practical utilization is limited because they cannot be operated in air owing to oxidation and high cost of the materials. Metal oxides are potential candidates for high temperature thermoelectric applications as they are thermally stable in air and show excellent durability. In particular, zinc oxide (ZnO) has been investigated as *n*-type thermoelectric material for high temperature applications because of better conversion efficiency compared to other oxides, abundance, non-toxicity and low cost.[3, 4]

The thermoelectric conversion efficiency of a material is closely tied to the dimensionless figure of merit zT

$$zT = \frac{\alpha^2 \sigma}{\kappa} T \quad (1)$$

where α, σ, κ and T denote respectively the Seebeck coefficient, the electrical conductivity, the thermal conductivity and the absolute temperature.

The thermoelectric efficiency can be enhanced by maximization of the power factor ($\alpha^2\sigma$) and reduction of the thermal conductivity. The power factor can be optimized by band gap engineering[5, 6] or doping. However, the most common approach for the figure of merit enhancement is to reduce the total thermal conductivity. Particularly, the lattice contribution by nanostructuring and nanoprecipitates in the matrix[7, 8, 9]; thereby, creating abundant grain boundaries, which scatter phonons more strongly than the electronic charge carriers.

For using nanostructured materials in thermoelectric devices, bulk solids are required. One of the methods to create bulk nanostructured materials is the *bottom-up* approach in which nanoparticles are compacted into the bulk material. Chemical vapour synthesis (CVS) is a facile method for the continuous production of nanoparticles that can be up-scaled to

industrial levels.[10] The CVS route is advantageous for tailoring the powder properties such as particle diameter, size distribution, morphology, crystallinity and doping concentration. Sintering of nanoparticles offers a promising route for the synthesis of bulk samples with nanoscale constituents. However, the challenge during the sintering process is to limit grain growth and to preserve a high density of grain boundaries. Pulsed electric current sintering (PECS) is a rapid sintering technique in which pulsed electric current and uniaxial pressure are simultaneously applied. It has been successfully demonstrated to manufacture bulk nanoscaled bodies.[11]

In this work, we report the high temperature electrical and thermal properties of Al-doped ZnO (AZO) nanocomposites. The AZO nanoparticles are prepared by the CVS route, which are then processed into bulk nanocomposites using PECS. The structural and thermoelectric properties of the sintered ceramic pellets are characterized. This study demonstrates the impact of the processing technique on the incorporation of a high amount of electrically active Al-dopant as reflected in the high value of electrical conductivity about 10^5 S/m and low Seebeck coefficient of about -50 μV/K at room temperature. In addition, the thermal conductivity is drastically decreased to an extremely low value of 1.0 W/mK at ambient temperature. In light of the obtained data, we discuss how the doping, nano-micro-structure and composite phase-mixture of ZnO and $ZnAl_2O_4$ in the sintered samples affect the charge transport, and in turn, the thermoelectric performance of AZO nanocomposites.

Experimental details

Synthesis of Nanoparticles

ZnO and AZO nanoparticles are prepared by CVS using a hot-wall reactor. The setup consists of a precursor delivery unit, a hot wall reactor and a thermophoretic particle collector. The

setup is described in detail elsewhere.[12, 13] The precursor unit comprises of two bubblers filled with liquid precursors, diethylzinc (DEZn) and triethylaluminium (TEAl) and are placed in a temperature-controlled oil bath to adjust the vapour pressure of the precursors. The precursors DEZn and TEAl are transported into the reactor chamber using helium as a carrier gas. Oxygen acting as a reaction gas with a flow rate of 1000 sccm (standard cubic centimetre per minute) is added to the helium/precursor mixture just before the gas mixture enters the reactor to avoid preliminary oxidation of the precursors. Thermal mass flow controllers are used to control the flow rates of the gases. The reactor consists of a ceramic alumina tube heated by a tube furnace. The synthesis temperature equal to the wall temperature of alumina tube is fixed at 1173 K. The precursors and oxygen react in the reaction zone to form oxide particles, which are subsequently transported to the thermophoretic particle collector by the gas stream. AZO powders are prepared by adjusting the desired mass flow of the DEZn and TEAl vapours, which is achieved by altering the oil bath temperatures and the helium flow rates through the precursors corresponding to nominal doping concentration of 0, 0.5, 1, 2 and 8 at% Al in the particles. In the collector, a thermophoretic force acts on the particles due to the temperature gradient between the hot quartz lamps and the water-cooled wall of the collector, where the particles are finally deposited. The powder is mechanically removed from the wall by a scraper. The process pressure maintained at 20 mbar is controlled by a butterfly valve and measured by a capacitive absolute pressure gauge placed at the outlet of the reactor.

Processing to Bulk Nanocomposites

The compaction of AZO and ZnO nanopowders into bulk nanocomposites is achieved using the PECS technique. A FCT HP D5/2 (FCT Systeme GmbH, Rauenstein, Germany) instrument is used for sintering. The powder is loaded into a graphite die with an inner diameter of 20 mm fabricated from high strength graphite. A graphite foil coated with boron nitride (BN) is used to avoid contact of the powder with the inner surface of the die. BN is

used as a high temperature electrical insulator that ensures the current flows through the powder and not through the dies during sintering. In order to reduce the radial temperature gradient in the dies and to minimize radiation heat losses, the complete die assembly is surrounded with carbon wool. The nanopowders are pre-pressed at 12 MPa and heated by a pulsed electric current with a heating rate of 100 K/min to the desired sintering temperature. A pulse pattern of 10:5 (10 ms on and 5 ms off) is used for sintering the samples. The samples are sintered at 700°C or 900°C with a holding time of 3 minutes. A uniaxial pressure of 35 MPa is applied to the specimens over the entire heating and cooling cycle. The samples are cooled down to 500°C with a cooling rate of 100 K/min. Further, the samples are furnace cooled to room temperature with a continuous release of applied pressure. The heating power is adjusted using a pyrometer, which monitors the temperature at the bottom of the upper graphite push-punch. The whole sintering procedure is performed at 1 mbar Ar atmosphere. The graphite foils on the surface of sintered samples are removed by grinding.

Characterization

The phase composition, crystal structure and isotropic crystallite size of the as-prepared nanopowders and sintered nanocomposites are determined by X-ray diffraction (XRD) using a PANalytical X-ray diffractometer (X-Pert PRO) with Ni-filtered Cu Kα (0.154 nm) radiation detected by an X-Celerator detector. The data are measured in the range $2\theta = 20°\text{-}120°$ and analyzed by Rietveld refinement using the software MAUD.[14] The geometric density of the sintered samples is determined from the sample mass and geometry. The nano-micro-structure and elemental analysis of the as-synthesized powders and sintered pellets are characterized by a high-resolution scanning electron microscope (SEM, JEOL-JSM 7500 F) using a scanning transmission detector (STEM) and equipped with an energy dispersive X-ray analyser (EDX, QX200 Bruker Quantax 2000).

The electrical conductivity and the Seebeck coefficient of the sintered nanocomposites are measured in He-atmosphere at 100 mbar using a ZEM-3 from Ulvac-Riko, Inc. The thermal conductivity is determined by the laser flash method using a LFA 457 Microflash from Netzsch-Gerätebau GmbH under atmospheric pressure with a flow of 75 sccm N_2. Due to the limited sample geometry within the available measurement techniques, the thermal transport is measured parallel to the direction of the pressing force and the sintering current, whereas the electrical transport is characterized perpendicular to this direction. This has to be taken into account when both transport processes are considered in combination.

Results and Discussion

Microstructure of nanoparticles and nanocomposites

Figure 1 depicts the XRD patterns of as-synthesized ZnO nanoparticles doped with 0, 0.5, 1, 2 and 8% of Al. The patterns show that the doped and undoped particles exhibit the hexagonal wurtzite structure and are single phase. It has been reported that the thermodynamic solubility limit of Al in ZnO is below 1%[15, 16]. Even though in the present study the doping exceeded the solubility limit we do not observe a second phase in the as-prepared nanopowders. This could be due to the CVS method, which is a non-equilibrium process, and therefore, allows to incorporate more dopant than permitted by the thermodynamic limit.[12, 13] The continuous increase in the broadening of XRD signals with increasing Al concentration (see Fig. 1) indicates that the crystallite size of the particles decreases. Both the crystallite size and the microstrain are determined from the Rietveld refinement of the data and are plotted as a function of Al concentration in Fig. 2. The addition of Al as dopant hinders the growth rate of the nanoparticles due to impurity drag, which results in smaller crystallites. It is also seen from Fig. 2 that the lattice microstrain increases with Al concentration indicating that Al is incorporated into the ZnO lattice. The findings are in agreement with previous studies.[17, 18]

Figure 3 shows the STEM micrograph of undoped ZnO nanopowders, which consists of nearly spherical crystalline particles with a small degree of agglomeration and a mean diameter of 15 nm substantiating the XRD data.

The XRD patterns of undoped and 8% Al-doped pellets sintered at 900°C are shown in Fig. 4. As is evident by the narrower Bragg reflections, substantial grain growth has occurred during sintering. Most of the Bragg reflections for the AZO nanocomposites belong to the hexagonal wurtzite phase similar to that of undoped ZnO. Also, the patterns reveal the presence of $ZnAl_2O_4$ spinel phase (gahnite). This additional phase is observed in the patterns when the nanocomposites have Al-concentration above ≥1% and the sintering temperature is 900°C. The XRD pattern of undoped ZnO sintered at 900°C shows strong texturing. The intensity of the (0002) reflection is strongly decreased while for the (10 $\bar{1}$0) reflection the intensity is increased compared to undoped nanoparticles. This indicates a preferential growth along the c-axis of the crystals[19] suggesting that the external applied pressure and the pulsed current during sintering defines the texture direction. The addition of Al as dopant in the nanocomposites enhances the intensity of (0002) reflection in comparison with (10 $\bar{1}$0) reflection as seen in Fig. 4 indicating a change in the anisotropy of the surface enthalpy of the particles, which modifies the growth direction and dynamics with the presence of Al in the samples.[20, 21]

Figure 5 shows SEM micrographs of the fresh fracture surface of AZO nanocomposites. The structure of undoped ZnO sintered at 900°C shows a grain size of 1-2 μm having a hexagonal cross section with intense faceting in the material. The faceting substantiates the XRD observation of a preferred growth along the c-axis of ZnO lattice. The hexagonal cross sectional structures are created due to the lower energy associated with these facets.[20] The micrographs for AZO nanocomposites reveal that ZnO grains are interspersed with the spinel $ZnAl_2O_4$ phase, which precipitates at the ZnO grain boundaries. The presence

of Al in the nanocomposites inhibits the growth of ZnO grains and the average size is confined in the range of 80-200 nm. The size of $ZnAl_2O_4$ precipitates is of the order of 10-50 nm. The grain growth for both ZnO and $ZnAl_2O_4$ depends on the sintering temperature as well as on Al-concentration in the material. Grain/crystallite growth is restricted due to Al-doping not only during particle synthesis but also during sintering due to pinning of the grain boundaries.[17, 19] Additionally, the presence of Al changes the surface energy of the (0001) facet, which can give rise to twins and planar defects.[21] The morphology of the grains changes from hexagonal as observed for undoped ZnO (see Fig. 5a) to a plate/planar-like structure for AZO nanocomposites as shown in Figs. 5b-5d. The addition of Al suppresses the grain boundary mobility thus enabling the pores to stick to the moving boundaries during sintering. That is why most of the porosity is located in the vicinity of $ZnAl_2O_4$ precipitates as revealed in the SEM micrographs (see Figs. 5b, 5c and 5d). Such porous materials with fine grains may act as good thermoelectric materials because their thermal conductivity can be strongly reduced while not affecting too much the electrical conductivity. The EDX line-scan across a region particularly at a distance of 40-50 μm (see Fig. 5e) in 8% AZO sample shows an enhancement of Al- and O-concentration at the nanoprecipitates-region consistent with the formation of $ZnAl_2O_4$ substantiated by the XRD pattern of sintered pellets (see Fig. 4).

The bulk relative density of the sintered samples is in the range of 65-93 %. The density of the specimens is affected both by the sintering temperature and Al-concentration in the samples. Increasing amounts of Al in the material as well as high sintering temperatures create more $ZnAl_2O_4$ precipitates. This makes the densification increasingly difficult due to the difference in the physical properties of $ZnAl_2O_4$ and ZnO. This observation is in agreement with previous findings in the literature.[22]

Dependence of transport properties of nanocomposites on Al-concentration

The room temperature electrical conductivities of nanocomposites sintered at 700°C and 900°C as a function of Al-concentration are illustrated in Fig. 6. The undoped ZnO sample sintered at 900°C has a room temperature electrical conductivity of $3*10^3$ S/m. Addition of 0.5% Al enhances the conductivity by two orders of magnitude to $1.5*10^5$ S/m. The substitution of Zn^{2+} by Al^{3+} increases the free charge carrier concentration to compensate for the electrical charge balance and in turn the electrical conductivity of the sample.[17, 23] This value is one of the highest for ZnO nanocomposites and is comparable to the bulk value of about $2*10^5$ S/m.[24, 25] In contrast; Nam *et al.* reported the electrical conductivity of about $1.3*10^4$ S/m for ZnO nanocomposites.[26] This indicates that with our processing method we are able to prepare nanocomposites incorporating active dopant in the material. On further addition of Al, the conductivity decreases very little for the samples sintered at 900°C.

The samples sintered at 700°C exhibit lower electrical conductivity compared to those sintered at 900°C and their conductivity decreases in a similar fashion with increasing Al-concentration (see Fig. 6). First, an increasing fraction of the non-conductive $ZnAl_2O_4$ phase reduces the volume available for the charge transport. Second, we suggest that smaller AZO grains-, and more $ZnAl_2O_4$ precipitates in the samples with higher Al-concentration increase the scattering of charge carriers, decreasing their mobility and in turn the electrical conductivity. This suggestion is in accordance with the microstructural observation (see Figs. 5a-5d). Besides the mobility, the other main factor for electrical conduction, namely the charge carrier concentration originating from electrically active dopant, is not directly obtainable from microstructural data and will be discussed below.

The impact of high electrical conductivity values is also observed in the Seebeck coefficient of the nanocomposites. Figure 7 illustrates how the Seebeck coefficient varies with Al-doping for nanocomposites sintered at 700°C and 900°C. The measured values of Seebeck coefficients are negative for all the samples indicating *n*-type conduction. The room

temperature Seebeck coefficient of the undoped ZnO sample sintered at 900°C is about -280 μV/K, which is in agreement with the relatively low electrical conductivity of this sample. As anticipated, with Al-doping the absolute value of the Seebeck coefficient decreases and reaches a value of about -50 μV/K at 0.5% Al. Further addition of Al has not much impact on the values of the Seebeck coefficient for the samples sintered at 900°C. As mentioned earlier, Al-doping results in the increase of charge carrier concentration by substitution of Zn by Al at the Zn-site, but this effect is confined by the low solubility limit. Interestingly, even though the electrical conductivities of the samples sintered at 700 °C and 900°C are remarkably different (see Figs. 6 and 7), their Seebeck coefficient values are very similar confirming the assumption of Kinemuchi *et al.*[4] and Nam *et al.*[26] that the impact of grain boundaries in the nanocomposite is less significant on the Seebeck coefficient than on the electrical conductivity. It is worth noting though that we observe a local minimum in the room temperature Seebeck coefficient at 1% Al-doping for both sintering temperatures. In case of the sample sintered at 700°C, the electrical conductivity decreased only slightly compared to the sample with 0.5 Al%-doping, the power factor reaches a maximum value at this dopant concentration amongst the samples sintered at 700°C.

The impact of the nanostructure on the thermal conductivity of sintered samples is enormous. Figure 8 illustrates how the room temperature thermal conductivity of samples sintered at 700°C and 900°C varies as a function of Al-content. Undoped ZnO sintered at 900°C exhibits a room temperature thermal conductivity of about 40 W/mK similar to the bulk value.[3, 27, 28] This is expected as the specimen contains grains in the micrometer range (see Fig. 5a) much larger than the mean free path of about 30 nm for phonons in ZnO.[29, 30] Addition of Al in the ZnO nanopowders decreases the thermal conductivity of the sintered nanocomposites. The amount of reduction in thermal conductivity depends on the sintering temperature and Al-content. In case of the samples sintered at 900°C, the thermal conductivity decreases with increasing Al-content, reaching its minimum of 7 W/mK at 8% Al-doping. However, the

samples sintered at 700°C exhibit much lower values and have a pronounced minimum at a doping concentration of 1% Al. The thermal conductivity of this sample is reduced by a factor of 40 compared to the bulk and reaches a value of about 1.0 W/mK, which is one of the lowest reported for oxide materials. Our findings on the low thermal conductivity of nanocomposites are in agreement with recently reported observation on AZO thin films by Loureiro *et al*.[31]. Kinemuchi *et al*.[4, 29] have reported that the thermal conductivity in ZnO nanocomposites can reach values below 5 W/mK when the grain size is around 50 nm, whereas Nam *et al.*[26] found reduction already for grain sizes below 200 nm. Since the phonon mean free path in ZnO is approximately 30 nm[29, 30], our findings of a strong reduction in the thermal conductivity for grain size of ZnO in the range of 50-100 nm agree well with these reported values. The smaller grains of $ZnAl_2O_4$ (10-30 nm, see Figs. 5c, 5d and 8) also have a major impact on the decrease of thermal conductivity. We attribute such a strong reduction in the total thermal conductivity to a reduction in lattice contribution by increased phonon scattering from $ZnAl_2O_4$ precipitates, point defects, porosity and refined nanograins by Al-doping.

Dependence of transport properties of sintered samples on temperature

As a representative exemplar for illustrating and discussing the charge transport of doped nanocomposites we use 1% AZO sample and compare it with the undoped specimen. The Seebeck coefficient α of nanocomposites as a function of measuring temperature is illustrated in Fig. 9 for undoped and 1% AZO nanocomposites sintered at 700°C and 900°C. For the undoped ZnO specimen sintered at 900°C, the Seebeck coefficient has large negative values in the range of -280 to -350 μV/K indicating a low charge carrier concentration. On the other hand, the Al-doped samples exhibit a low absolute value of the Seebeck coefficient over the complete temperature interval pointing out the enhancement in concentration of free charge carriers as discussed before. As illustrated in Fig. 9, the Seebeck coefficient decreases with

temperature in agreement with the findings in the literature for bulk doped ZnO ceramics.[3, 32-34] Similar results were also reported for doped nanocomposites.[4, 26, 29]

The temperature dependence of the Seebeck coefficient of a degenerate semiconductor can be described using Jonker and Pisarenko relationship[8] as expressed in Eq. (2)

$$\alpha = \frac{8\pi^2 k_B^2}{3eh^2} \cdot m^* \left(\frac{\pi}{3 \cdot n} \right)^{2/3} T \qquad (2)$$

where n is the charge carrier concentration and m^* is the effective mass at the Fermi level. The remaining parameters are natural constants: h is the Planck constant, e is the elementary charge and k_B is the Boltzmann constant. Eq. (2) clearly shows that a higher charge carrier concentration n causes a decrease in α provided m^* and T remain constant, which explains the tendency observed in Fig. 7. Also, Eq. (2) shows that the Seebeck coefficient should vary linearly with temperature as illustrated in Fig.9 provided m^* and n are constant in the temperature interval. The charge carrier concentration n can be evaluated by fitting the data in Fig. 9 for doped samples with Eq. (2) and using $m^* = 0.33\ m_e$, where m_e is the electron rest mass.[26] In case of the samples sintered at 700°C, the low temperature interval (300-670 K) is considered for evaluating the charge carrier concentration. It should be noted that this analysis yields the charge carrier concentration in the volume fraction of the conductive material.

The charge carrier concentration for different samples is plotted in Fig. 10. It can be seen that the carrier concentration in all the sintered samples is quite high with values on the order of 10^{20} cm^{-3}, satisfying the criterion of degeneracy. For those samples sintered at 900°C, we find values that are a factor of 3 to 4 larger than for the samples sintered at 700°C indicating that at higher sintering temperature more Al is incorporated into ZnO lattice. Considering the amount of Al-dopants, the carrier concentration is of the same order as the theoretical concentration[35] for 0.5% Al underlining the effectiveness of our synthesis route to prepare highly doped material (see Fig. 10 and reference[35]). For higher Al-contents the evaluated carrier concentration is different from the theoretical Al-content indicating only a limited fraction of

added Al might be effective as dopant and the remaining Al is precipitated as $ZnAl_2O_4$ spinel phase as demonstrated by XRD and SEM micrographs of sintered samples.

Figure 11 shows the temperature dependence of the electrical conductivity σ of the undoped and 1% AZO nanocomposites. All samples exhibit decreasing electrical conductivity with increasing temperature indicating a metallic or strongly degenerate behaviour. It should be noted that even for undoped ZnO we observe the same tendency albeit the absolute values are much lower than for the Al-doped samples.

The electrical conductivity can be expressed as

$$\sigma = ne\mu_e \quad (3)$$

where, μ_e is the average mobility of charge carriers in the total volume of the material.

Taking into account Eq. (3) and the charge carrier concentrations from Fig. 10, the room temperature mobility of the charge carriers can be evaluated from the electrical conductivity. By dividing the evaluated average mobility of the charge carriers with the relative density of the samples, we obtain a normalized mobility value for the charge carriers. This normalized mobility takes into account the electrically active volume of the samples and more directly reflects the influence of the nano-micro-structure on the transport of the charge carriers. The normalized mobility is illustrated for the room temperature values as a function of Al-content in Fig. 12. The mobility of the charge carriers in sintered nanocomposites decreases with increasing Al-doping in the material irrespective of the sintering temperature in agreement with previous reports.[35, 36, 37] At room temperature, the mobility of charge carriers in most of the samples is well in the range of undoped and Al-doped polycrystalline bulk ZnO (20 to 80 cm^2/Vs)[35] and pulsed laser deposited thin films (30 to 10 cm^2/Vs, decreasing with increasing Al-content).[37] However, it should be mentioned that Baxter *et al.*[38] reported higher mobility values for undoped ZnO thin films and nanowires and showed that annealing

enhances the mobility of charge carriers (140-230 cm^2/Vs). The high mobility found for the sample with 0.5% Al-content sintered at 900°C (46 cm^2/Vs) suggests that even though this sample has grains of about 200 nm and the spinel $ZnAl_2O_4$ phase is present as observed from the structural evaluation, the microstructure has little influence on the transport of the charge carriers in this sample. A further increase of the Al-content, however, increases the amount of $ZnAl_2O_4$ nanoprecipitates, which scatter the charge carriers thereby decreasing the mobility. In case of the samples sintered at 700°C, the lower mobility values indicate that the microstructure of specimens contains smaller grains and concurrently, an increased fraction of grain boundaries scatters the charge carriers more effectively (see Figs. 5c and 5d). We cannot directly correlate that the increase in volume fraction of the spinel $ZnAl_2O_4$ phase with Al-doping is solely responsible for the mobility reduction and in turn the electrical conductivity as the amount of the spinel phase is much less than the observed diminution in mobility of sintered nanocomposites. As already seen from the dependence of Seebeck coefficient and electrical conductivity on the doping concentration, we also find from their dependence on temperature that the nanostructure and composite nature has an impact on the electrical conductivity, but not on the Seebeck coefficient of the sintered samples, supporting the hypothesis by Nam *et al.*[26]

The thermal conductivity κ of the nanocomposites is shown in Fig. 13. It decreases rapidly with temperature for undoped ZnO as also reported by Ohtaki *et al.*[3] Doping with Al not only reduces strongly the thermal conductivity of the samples but also modifies the temperature dependence of κ as illustrated for 1% Al-doped specimen. It can be also seen that the sample sintered at 700°C with 1% Al-content displays the lowest κ of all the measured specimens and its behaviour is temperature independent. Kinemuchi *et al.*[4, 29] observed a similar dependence of κ on grain size and temperature. We attribute that phonon-phonon scattering is responsible for the decrease in thermal conductivity with increasing temperature

in the case of undoped ZnO.[35, 39] Additionally, in the case of the Al-doped nanocomposites, significant reduction in phonon transport occurs by grain boundary scattering at ZnO nanograins, $ZnAl_2O_4$ precipitates, point defects and pores present in the sample.[29, 36, 39] We estimate the electronic contribution κ_e to the total thermal conductivity using the Wiedemann-Franz law, $\kappa_e = L\sigma T$, where L is the Lorenz number ($2.44*10^{-8}$ V^2/K^2).[40] The electronic contribution to the thermal conductivity κ_e amounts to about 8-43% at 900 K for all the measured samples implying the major contribution in the total thermal conductivity is due to the lattice conductivity κ_L. Hence, the nanocomposite microstructure of the samples strongly influences the thermal conductivity and we are able to reduce the lattice contribution to the total thermal conductivity drastically as reflected in the low κ values and rising contribution from electronic carriers to the thermal conductivity.

Thermoelectric figure of merit

The numerical values for the dimensionless figure of merit *zT* resulting from the calculation using Eq. (1) are shown in Fig. 14. These values have to be taken with care because thermal and electrical transport was measured in perpendicular directions. However, the dependence of *zT* on temperature features a quite smooth slope, and this behaviour is assumed to be rather insensitive against possible anisotropy within the sample, allowing for a comparison amongst our samples and with temperature dependent data reproduced from Jood *et al.*[36] Due to a massive increase in electrical conductivity above 850 K their *zT* shows a kink, whereas our samples exhibit a much smoother dependence of *zT* on temperature. A figure of merit that is high over a wide temperature range is advantageous for power generation in large thermal gradients. The highest value for *zT* of 0.24 at 965 K is calculated for nanocomposites doped with 1% Al sintered at 700°C as illustrated in Fig. 14. This sample exhibits a slightly higher absolute Seebeck coefficient than all other doped samples. Together with an only slight

decrease in the electrical conductivity compared to the sample with 0.5% Al-content sintered at 700°C, this results in the highest power factor amongst the samples sintered at 700°C and coupled with a strong reduction in the thermal conductivity results in the highest zT amongst all sintered nanocomposites.

We have demonstrated that nanostructuring and the composite nature of the material strongly affect the thermal and electrical transport due to the scattering of phonons and charge carriers at the grain boundaries and nanoprecipitates while only a minor influence is observed on the Seebeck coefficient because the concentration of active charge carriers does not vary a lot beyond the solubility limit of Al in ZnO. Still, the Al-content beyond the solubility limit can be used to tailor the nano-micro-structure in such a fashion that the lattice contribution to the thermal conductivity is largely reduced. In this way, we optimized the ratio of σ/κ to enhance zT of the material.

Conclusions

We synthesized Al-doped ZnO nanoparticles by chemical vapour synthesis in a hot wall reactor. The powders were compacted into bulk nanocomposites by pulsed electric current sintering. The structural characterization shows that the presence of Al-dopant inhibits grain growth both in the synthesized nanopowders and the sintered nanocomposites. The impact of Al-doping, nanograins/grain boundaries and $ZnAl_2O_4$ nanoprecipitates, i.e. the microstructure of the nanocomposites, on the thermoelectric properties are demonstrated. With our processing methodology we are able to create efficient Al-doping in ZnO, which give bulk-like electrical conductivity and strong reduction in the thermal conductivity in the nanocomposites at room temperature. We observed a strong correlation between microstructure and thermoelectric properties of the sintered nanocomposites. However, the

detailed mechanism of the impact of microstructure on the transport of charge carriers requires further investigations. With such knowledge, a further tuning of the thermoelectric properties would be possible.

Acknowledgements

The authors are thankful to Dr. Christian Notthoff, University of Duisburg-Essen, for SEM/EDX imagining. The authors gratefully acknowledge the financial support by the European Union and Ministry of Economic Affairs and Energy of the State North Rhine-Westphalia in Germany (Objective 2 Programme: European Regional Development Fund, ERDF). Also, financial support in the framework of a young investigator grant by the Ministry for innovation, science and research of the State North Rhine-Westphalia in Germany is gratefully acknowledged.

References

[1] Dresselhaus M. S.; Chen G.; Tang M.; Yang R.; Lee H.; Wang D.; Ren Z.; Fleurial J. P.; Gogna P. *Adv. Mater.* **2007**, *19*, 1043.

[2] Heremans J. P.; Thrush C. M.; Morelli D. T. *J. Appl. Phys.* **2005**, *98*, 063703.

[3] Ohtaki M.; Tsubota T.; Eguchi K.; Arai H. *J. Appl. Phys.* **1996**, *79*, 1816.

[4] Kinemuchi Y.; Nakano H.; Mikami M.; Kobayashi K.; Watari K.; Hotta Y. *J. Appl. Phys.* **2010**, *108*, 053721.

[5] He J.; Kanatzidis M. G.; Dravid V. P. *Materials Today* **2013**, *16*, 166.

[6] Heremans J. P.; Wiendlocha B.; Chamoire A. M. *Energy Environ. Sci*. **2012**, *5*, 5510.

[7] Kim W.; Wang R.; Majumdar A. *NanoToday* **2007**, *2*, 40.

[8] Snyder G. J.; Toberer E. S. *Nature Materials* **2008**, *7*, 105.

[9] Liu W.; Yan X.; Chen G.; Ren Z. *Nano Energy* **2012**, *1*, 42.

[10] Winterer M. *Nanocrystalline Ceramics: Synthesis and Structure*; Springer Verlag: Berlin, **2002**.

[11] Anselmi-Tamburini U.; Garay J. E.; Munir Z. A.; Tacca A.; Maglia F.; Spinolo G. *J. Mater. Res.* **2004**, *19*, 3255.

[12] Schilling C.; Zähres M.; Mayer C.; Winterer M. *J. Nanopart. Res.* **2014**, *16:2506*, 1.

[13] Hartner S.; Ali M.; Schulz C.; Winterer; Wiggers H. *Nanotechnology* **2009**, *20*, 445701.

[14] Lutterotti L.; Scardi P. *J. Appl. Crystallogr.* **1990**, *23*, 246 and MAUD (Material Analysis Using Diffraction) is a free Java program for Rietveld Analysis.

[15] Yoon M. H.; Lee S. H.; Park H. L.; Kim H. K.; Jang M. S. *J. Mater. Sci. Lett.* **2002**, *21*, 1703.

[16] Shirouzu K.; Kawamoto T.; Enomoto N.; Hojo J. *Jpn. J. Appl. Phys.* **2010**, *49*, 010201.

[17] Ingham B.; Linklater R.; Kemmitt T. *J. Phys. Chem. C* **2011**, *115*, 21034.

[18] Brehm J. U.; Winterer M.; H. Hahn *J. Appl. Phys.* **2006**, *100*, 064311.

[19] Clarke D. R. *J. Am. Ceram. Soc.* **1999**, *82*, 485.

[20] Wang Z. L. *J. Phys. Condens. Matter* **2004**, *16*, R829.

[21] Ding Y.; Kong X. Y.; Wang Z. L. *Phys. Rev. B* **2004**, *70*, 235408.

[22] Hong W. S.; De-Jonghe L. C.; Yang X.; Rahaman M. N. *J. Am. Ceram. Soc.* **1995**, *78*, 3217.

[23] Hauffe K.; Vierk A. L. *Z. Physik. Chem.***1950**, *196*, 160.

[24] Kinemuchi Y.; Ito C.; Kaga H.; Aoki T.; Watari K. *J. Mater. Res.* **2007**, *22*, 1942.

[25] Tsubota T.; Ohtaki M.; Eguchi K.; Arai H. *Proceedings of the 16th International Conference on Thermoelectrics (ICT 1997)* (IEEE, Piscataway **1997**) 240.

[26] Nam W. H.; Lim Y. S.; Choi S. M.; Seo W. S.; Lee J. Y. *J. Mater. Chem.* **2012**, *22*, 14633.

[27] Gadzhiev G. G. *High Temperature*, **2003**, *41*, 778.

[28] Vogel-Schäuble N.; Dujardin R.; Weidenkaff A.; Aguirre M. H. *J. Electron. Mater.* **2012**, *41*, 1606.

[29] Kinemuchi Y.; Mikami M.; Kobayashi K.; Watari K.; Hotta Y. *J. Electron. Mater.* **2010**, *39*, 2059.

[30] LeBlanc S.; Phadke S.; Kodama T.; Salleo A.; Goodson K. E. *Appl. Phys. Lett.* **2012**, *100*, 163105.

[31] Loureiro J.; Neve N.; Barros R.; Mateus T.; Santos R.; Filonovich S.; Reparaz S.; Sotomayor-Torres C. M.; Wyczisk F.; Divay L.; Martins Rodrigo; Ferreira I. *J. Mat. Chem. A.* **2014**, *2*, 6649.

[32] Kim K. H.; Shim S. H.; Shim K. B.; Niihara K.; Hojo J. *J. Am. Ceram. Soc.* **2005**, *88*, 628.

[33] Ma N.; Li J. F.; Zhang B. P.; Lin Y. H.; Ren L. R.; Chen G. F. *J. Phys. and Chem. of Solids* **2012**, *71*, 1344.

[34] Fujishiro Y.; Miyata M.; Awano M.; Maeda K. *J. Am. Ceram. Soc.* **2003**, *86*, 2063.

[35] Tsubota T.; Ohtaki M.; Eguchi K.; Arai H. *J. Mater. Chem.* **1997**, *7*, 85.

[36] Jood P.; Mehta R.; Zhang Y.; Peleckis G.; Wang X.; Siegel R. W.; Borca-Tasciuc T.; Dou S. X.; Ramanath G. *Nano Lett.* **2011**, *11*, 4337.

[37] Kim H.; Piqué A.; Horwitz J. S.; Murata H.; Kafafi Z. H.; Gilmore C. M.; Chrisey D. B. *Thin Solid Films* **2000**, *377-378*, 798.

[38] Baxter J. B.; Schmuttenmaer C. A. *J. Phys. Chem. B* **2006**, *110*, 25229.

[39] Toberer E. S.; Zevalkink A.; Snyder G. J. *J. Mater. Chem.* **2011**, *21*, 15843.

[40] Ohtaki M.; Araki K.; Yamamoto K. *J. Electron. Mater.* **2009**, *38*, 1234.

Figure captions

Figure 1: X-ray diffractograms of as-synthesized AZO nanopowders by the CVS method.

Figure 2: Evolution of crystallite size and microstrain as a function of the nominal Al-concentration for as-prepared AZO nanoparticles.

Figure 3: HRSEM micrograph (in STEM mode) of as-synthesized undoped ZnO nanoparticles.

Figure 4: X-ray diffractograms of undoped and 8% Al-doped ZnO nanocomposites sintered at 900°C by PECS.

Figure 5: SEM micrographs of fractured surfaces of (a) undoped and (b) 0.5 % AZO pellets sintered at 900°C; (c) 0.5%, (d) 1% AZO nanocomposites sintered at 700°C and (e) EDX line scan across a region containing $ZnAl_2O_4$ nanoprecipitates in 8% AZO sample sintered at 900°C.

Figure 6: Room temperature electrical conductivity as a function of Al-concentration for nanocomposites sintered at 700°C and 900°C.

Figure 7: Room temperature Seebeck coefficient as a function of Al-concentration for nanocomposites sintered at 700°C and 900°C.

Figure 8: Variation of room temperature thermal conductivity as a function of Al-concentration for nanocomposites sintered at 700°C and 900°C.

Figure 9: Temperature dependence of the Seebeck coefficient of nanocomposites sintered at 700°C and 900°C.

Figure 10: Room temperature charge carrier concentration as a function of Al-concentration for nanocomposites sintered at 700°C and 900°C. The carrier concentration was evaluated from the temperature dependence of the Seebeck coefficient and refers to the electrically active volume fraction.

Figure 11: Temperature dependence of the electrical conductivity of nanocomposites sintered at 700°C and 900°C.

Figure 12: Normalized room temperature mobility as a function of Al-concentration of nanocomposites sintered at 700°C and 900°C. The normalization takes out the contribution of electrically inactive volume fraction (pores), reflecting more directly the influence of the grain boundaries on the transport of the charge carriers. The average mobility in the total volume is lower.

Figure 13: Temperature dependence of the thermal conductivity of nanocomposites sintered at 700°C and 900°C.

Figure 14: Temperature dependence of the figure of merit *zT* for 1% AZO nanocomposites sintered at 700°C and 900°C. The present study is compared to data from Jood *et al.* (see reference[36]).

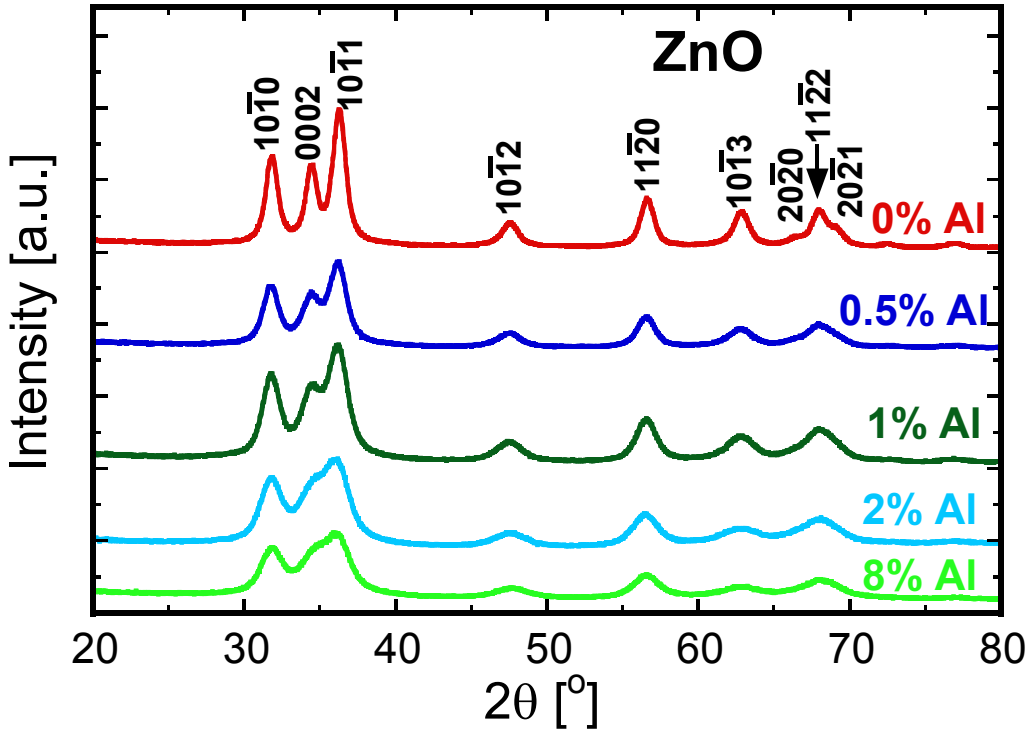

Figure 1: X-ray diffractograms of as-synthesized AZO nanopowders by the CVS method.

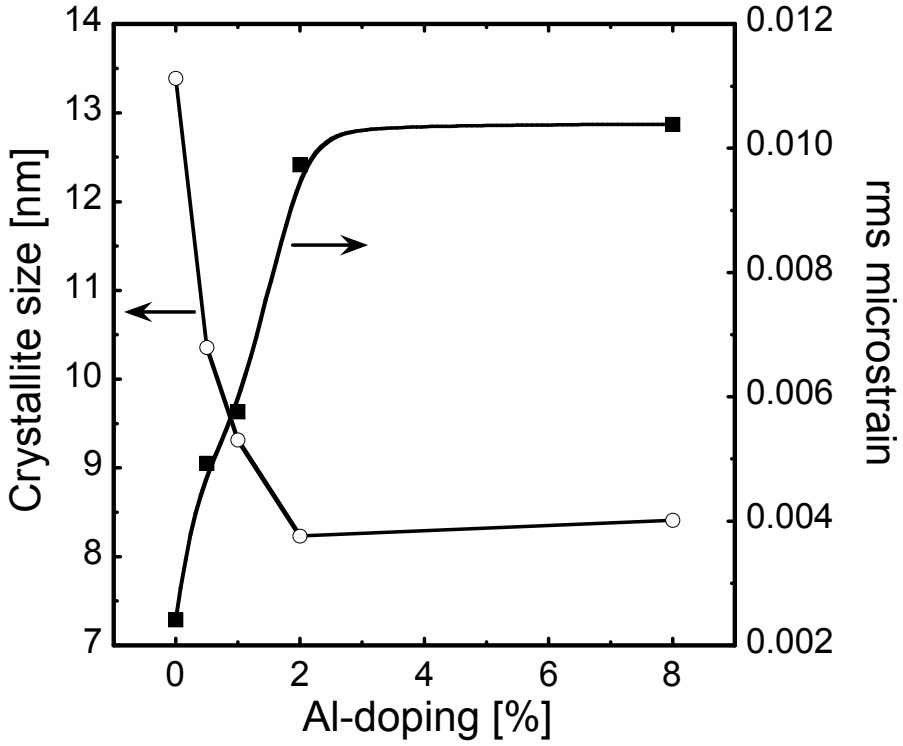

Figure 2: Evolution of crystallite size and microstrain as a function of the nominal Al-concentration for as-prepared AZO nanoparticles.

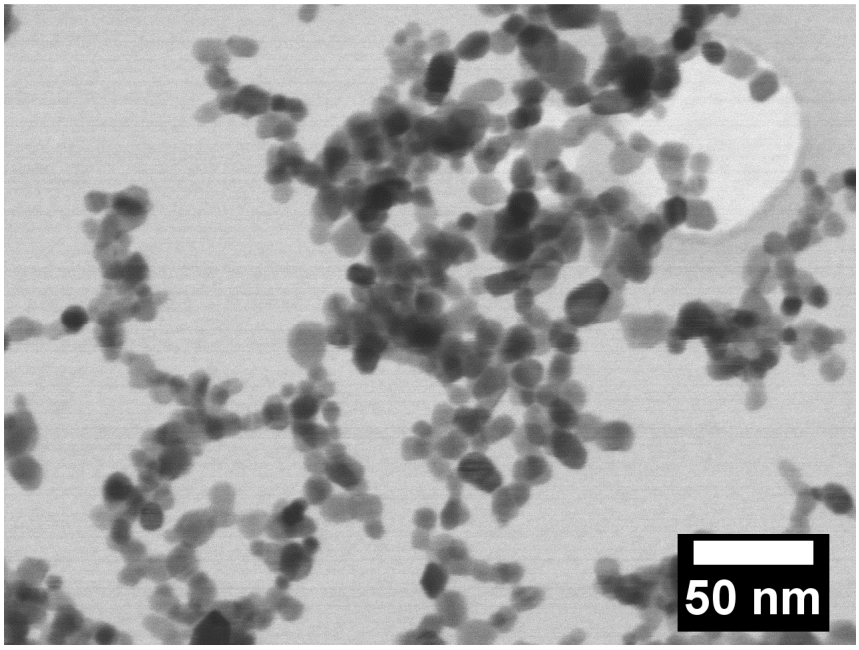

Figure 3: HRSEM micrograph (in STEM mode) of as-synthesized undoped ZnO nanoparticles.

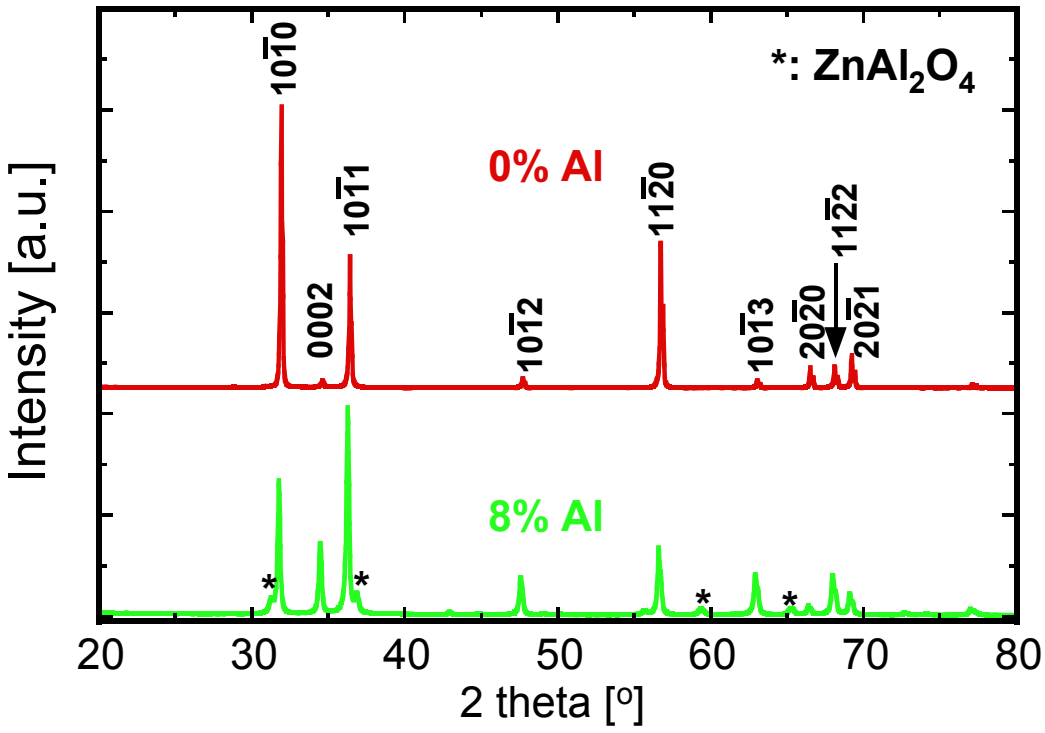

Figure 4: X-ray diffractograms of undoped and 8% Al-doped ZnO nanocomposites sintered at 900°C by PECS.

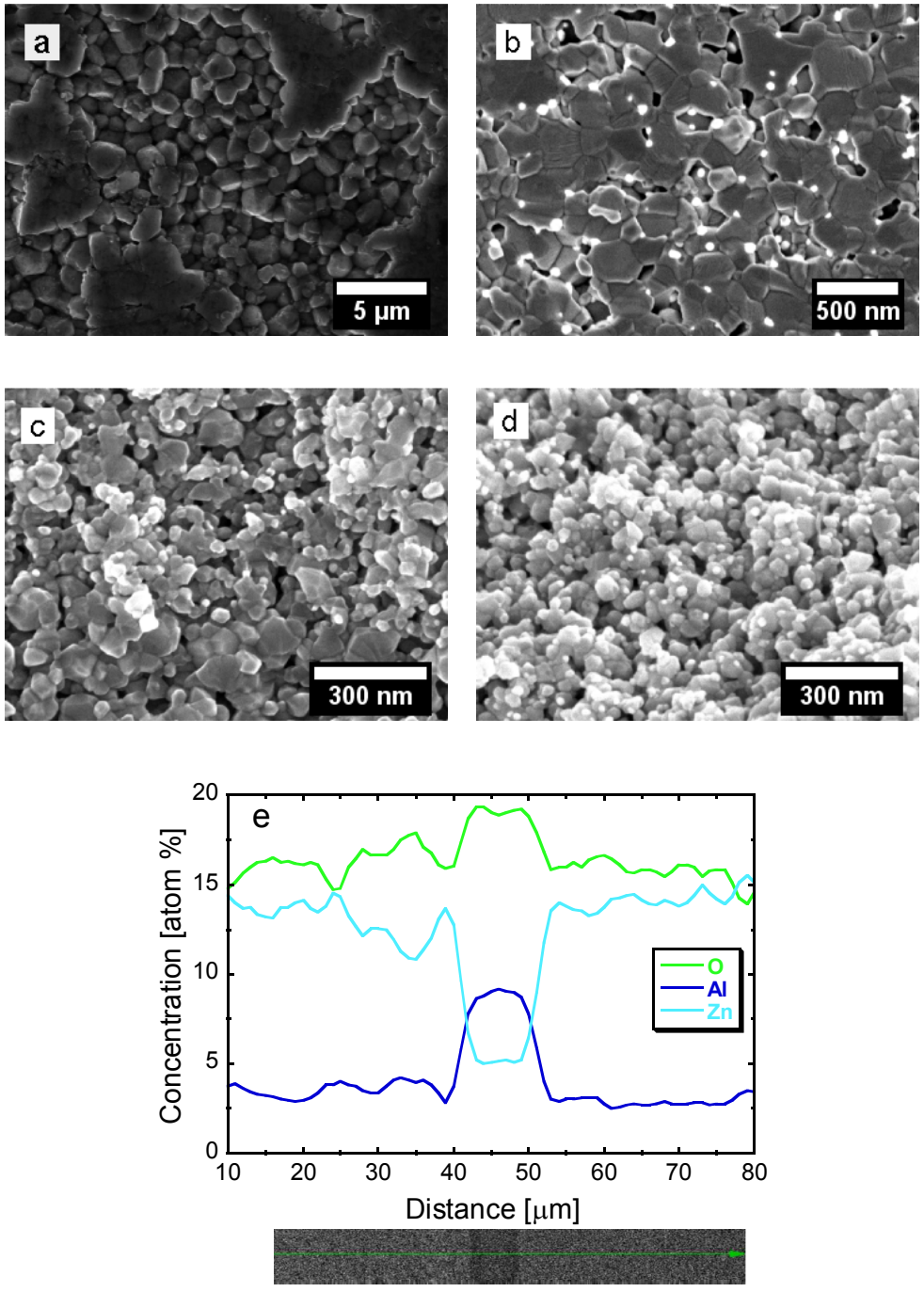

Figure 5: SEM micrographs of fractured surfaces of (a) undoped and (b) 0.5 % AZO pellets sintered at 900°C; (c) 0.5%, (d) 1% AZO nanocomposites sintered at 700°C and (e) EDX line scan across a region containing $ZnAl_2O_4$ nanoprecipitates in 8% AZO sample sintered at 900°C.

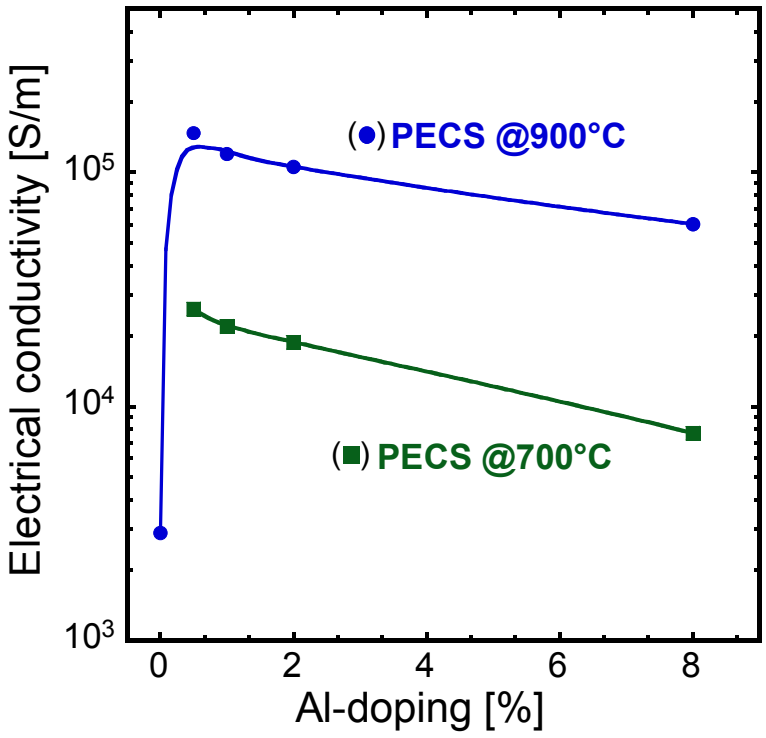

Figure 6: Room temperature electrical conductivity as a function of Al-concentration for nanocomposites sintered at 700°C and 900°C.

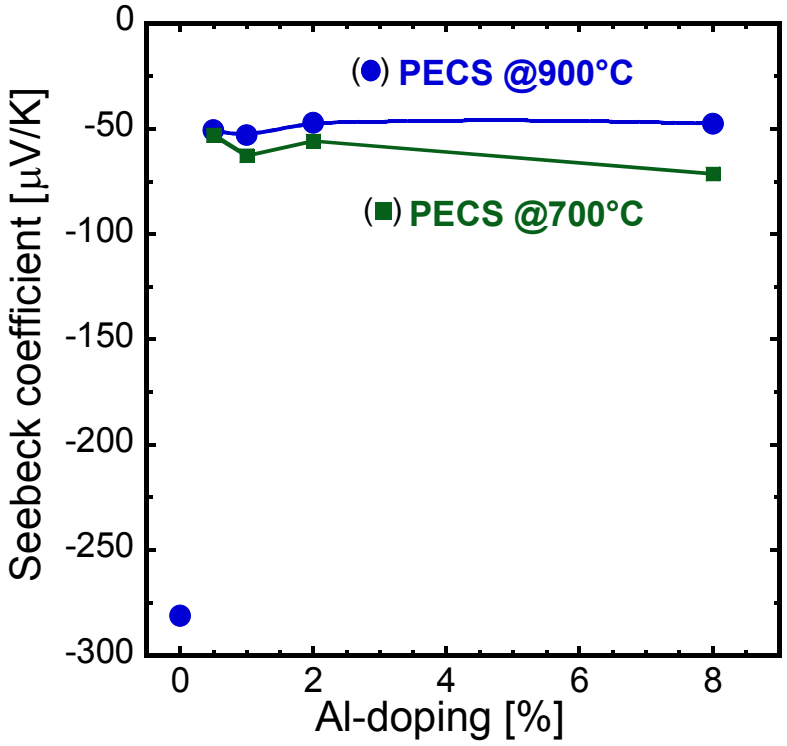

Figure 7: Room temperature Seebeck coefficient as a function of Al-concentration for nanocomposites sintered at 700°C and 900°C.

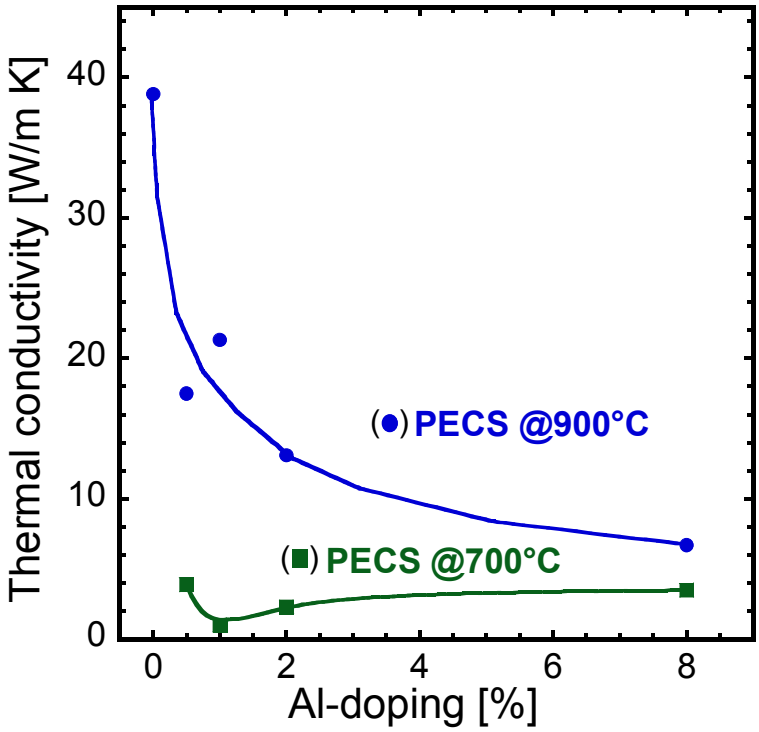

Figure 8: Variation of room temperature thermal conductivity as a function of Al-concentration for nanocomposites sintered at 700°C and 900°C.

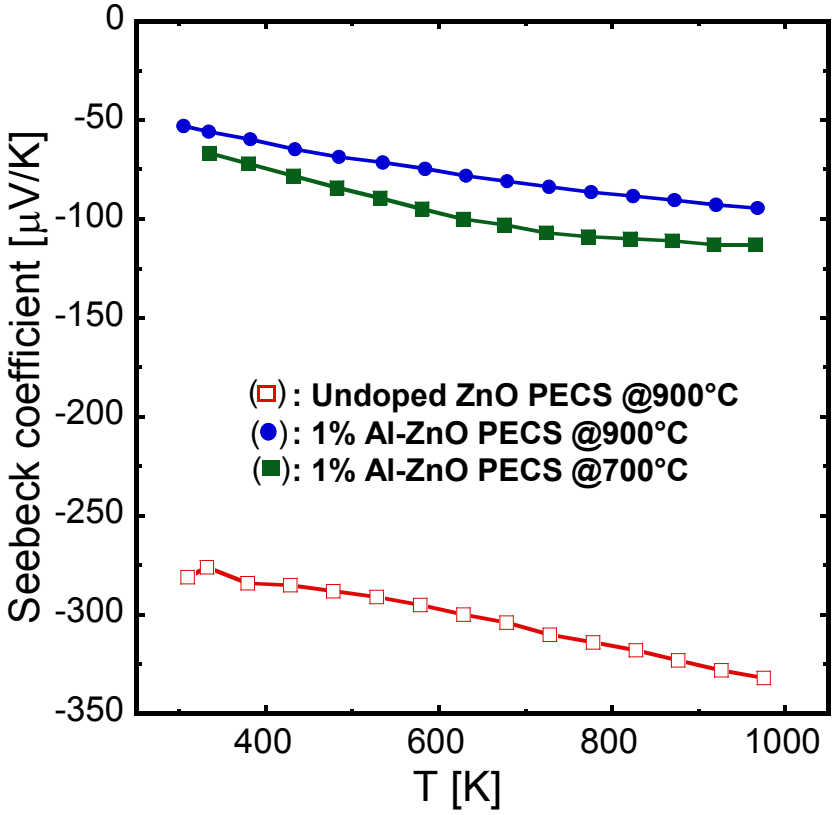

Figure 9: Temperature dependence of the Seebeck coefficient of nanocomposites sintered at 700°C and 900°C.

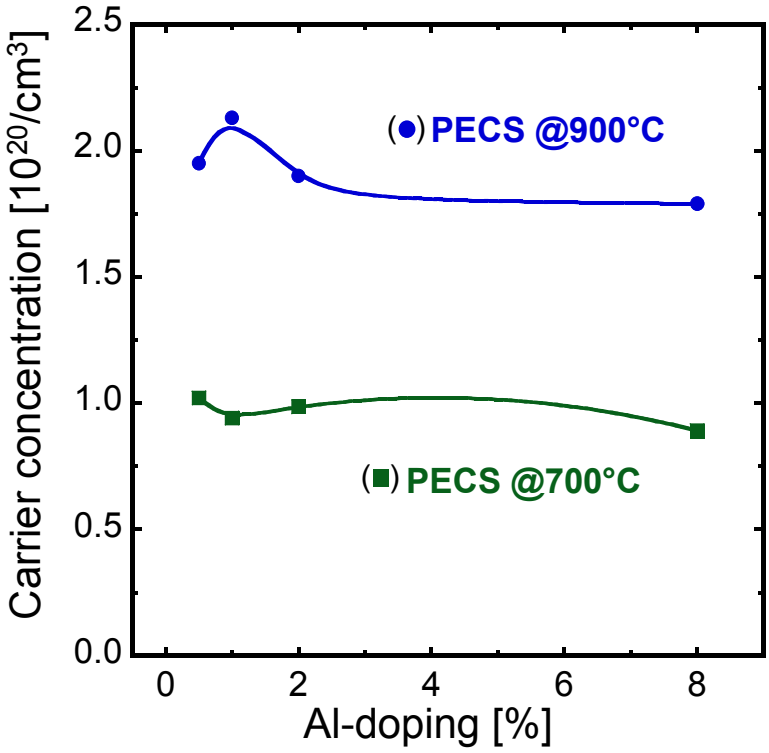

Figure 10: Room temperature charge carrier concentration as a function of Al-concentration for nanocomposites sintered at 700°C and 900°C. The carrier concentration was evaluated from the temperature dependence of the Seebeck coefficient and refers to the electrically active volume fraction.

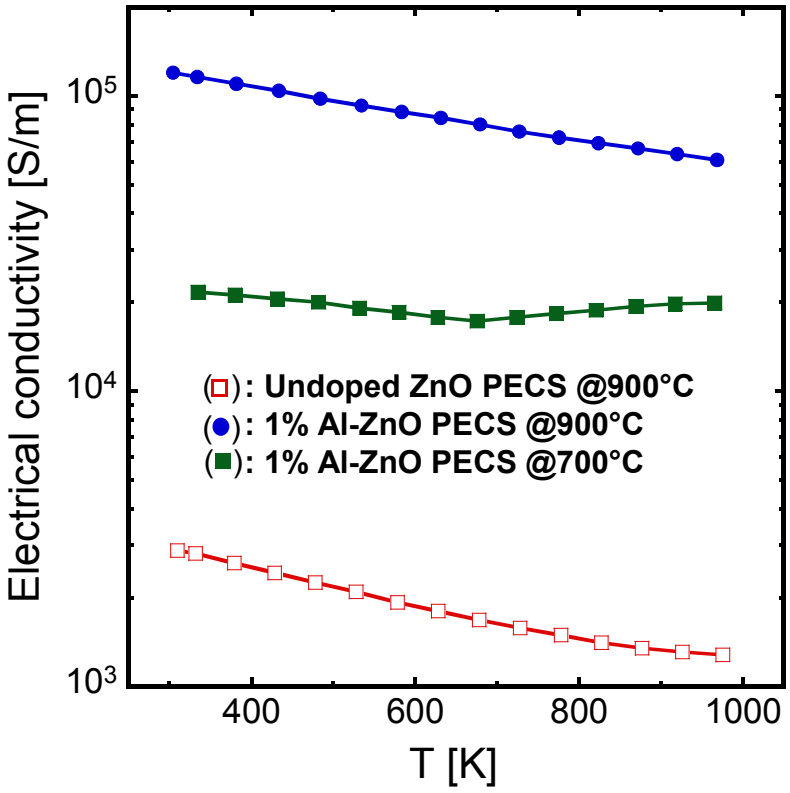

Figure 11: Temperature dependence of the electrical conductivity of nanocomposites sintered at 700°C and 900°C.

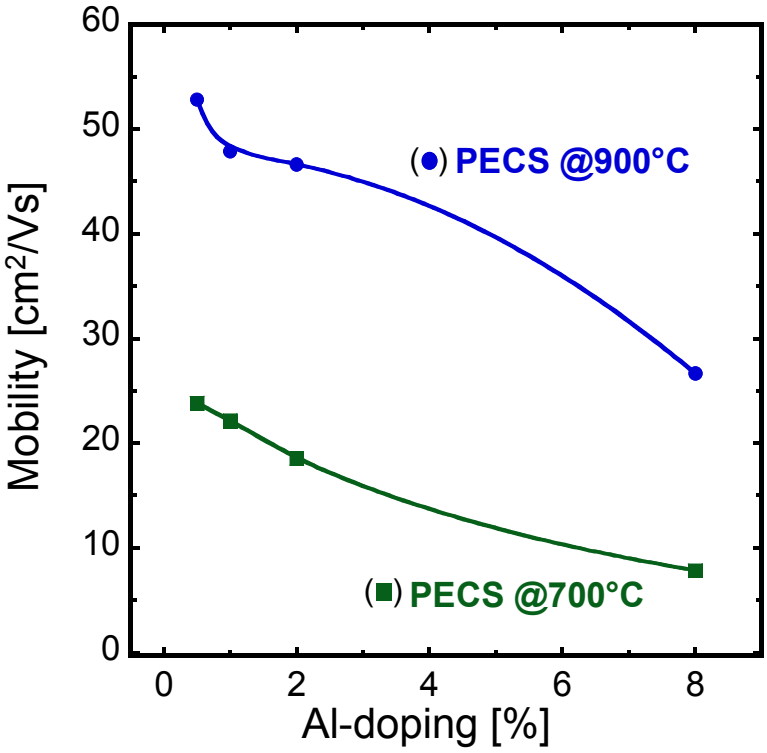

Figure 12: Normalized room temperature mobility as a function of Al-concentration for nanocomposites sintered at 700°C and 900°C. The normalization takes out the contribution of electrically inactive volume fraction (pores), reflecting more directly the influence of the grain boundaries on the transport of the charge carriers. The average mobility in the total volume is lower.

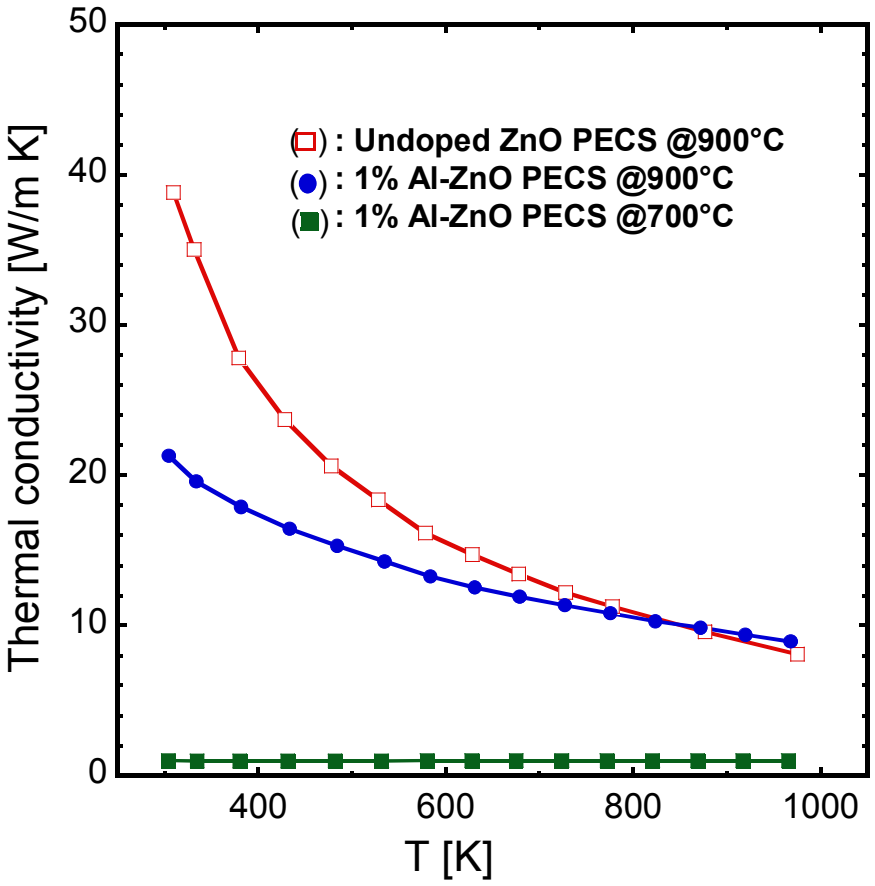

Figure 13: Temperature dependence of the thermal conductivity of nanocomposites sintered at 700°C and 900°C.

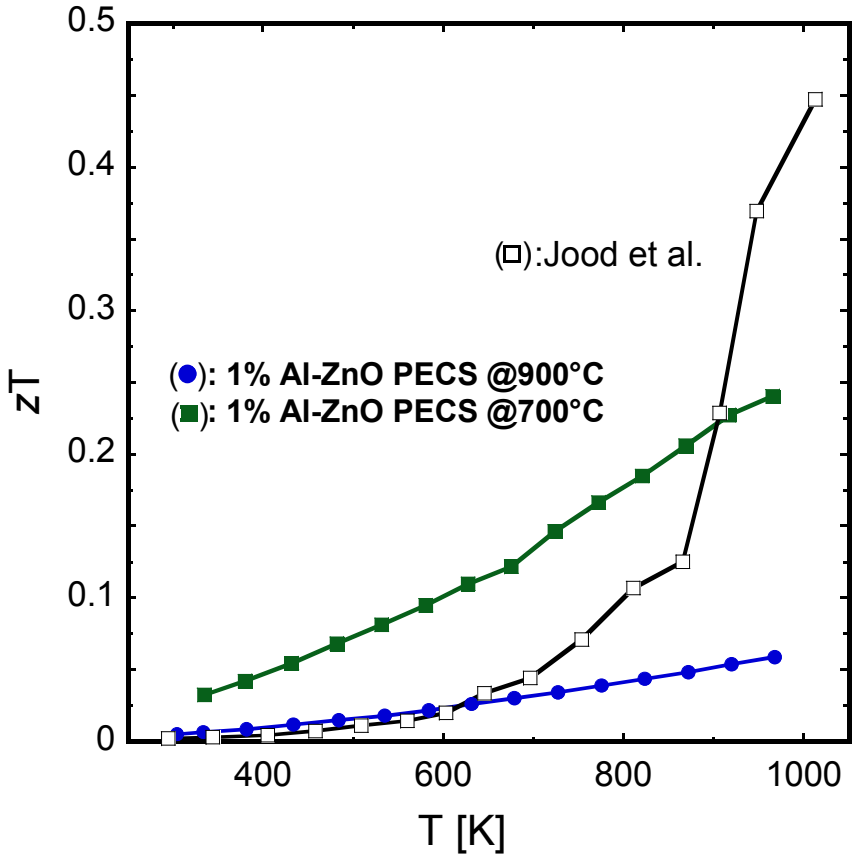

Figure 14: Temperature dependence of the figure of merit *zT* for 1% AZO nanocomposites sintered at 700°C and 900°C. The present study is compared to data from Jood *et al*. (see reference[36]).

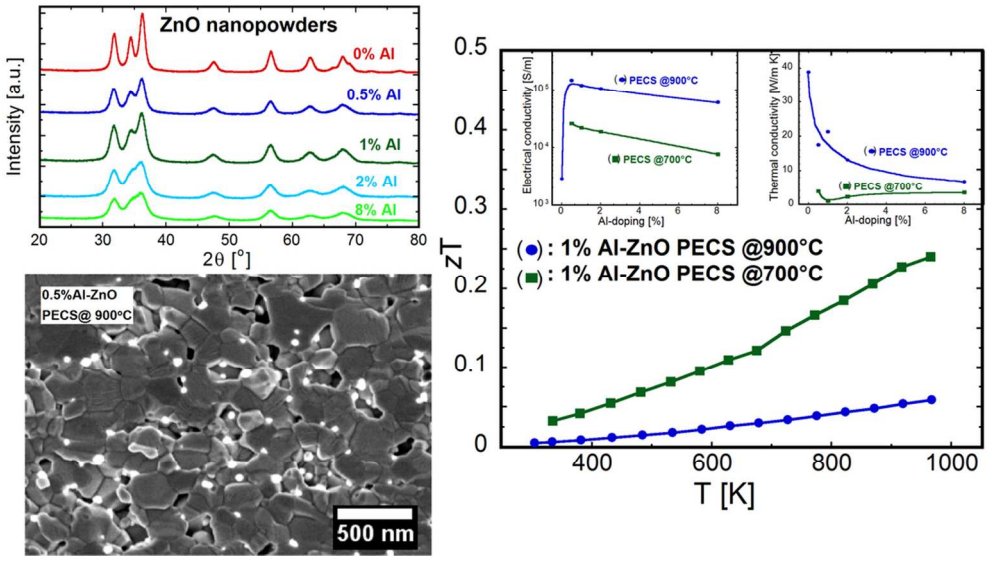

50x27mm (600 x 600 DPI)